

NDE and SHM Simulation for CFRP Composites

Authors : Cara A.C. Leckey
F. Raymond Parker

ABSTRACT

Ultrasound-based nondestructive evaluation (NDE) is a common technique for damage detection in composite materials. There is a need for advanced NDE that goes beyond damage detection to damage quantification and characterization in order to enable data driven prognostics. The damage types that exist in carbon fiber-reinforced polymer (CFRP) composites include microcracking and delaminations, and can be initiated and grown via impact forces (due to ground vehicles, tool drops, bird strikes, etc), fatigue, and extreme environmental changes. X-ray microfocus computed tomography data, among other methods, have shown that these damage types often result in voids/discontinuities of a complex volumetric shape. The specific damage geometry and location within ply layers affect damage growth. Realistic three-dimensional NDE and structural health monitoring (SHM) simulations can aid in the development and optimization of damage quantification and characterization techniques. This paper is an overview of ongoing work towards realistic NDE and SHM simulation tools for composites, and also discusses NASA's need for such simulation tools in aeronautics and spaceflight. The paper describes the development and implementation of a custom ultrasound simulation tool that is used to model ultrasonic wave interaction with realistic 3-dimensional damage in CFRP composites. The custom code uses elastodynamic finite integration technique and is parallelized to run efficiently on computing cluster or multicore machines.

Cara A.C. Leckey, Research Physicist
F. Raymond Parker, Research Scientist
Nondestructive Evaluation Sciences Branch, NASA Langley Research Center, Hampton, VA
23681

INTRODUCTION

Nondestructive evaluation (NDE) and structural health monitoring (SHM) techniques capable of quantifying and fully characterizing damage are needed for aerospace composites. The ability to fully characterize damage in carbon fiber reinforced polymer (CFRP) composite components is required to enable damage progression models capable of yielding accurate remaining life predictions. For example, the depth at which delaminations occur is directly related to how damage growth progresses [1]. Therefore, a ‘full’ characterization of delamination damage needs to go beyond a quantitative measure of the in-plane area (size) of the damage, to also include the depth/ply at which the damage occurs. For multilayered delamination damage, a full assessment would ideally include the depth and size of all delaminations, if possible. A ‘full’ damage characterization for other damage types may require different damage information. Microcracking may be best characterized by a measure of microcrack density correlated to depth through the material, while fiber waviness may require a statistical measure of the affected locations and corresponding ranges in the angle of unintended in-plane or out-of-plane alignment/waviness of fibers (i.e., a ‘waviness angle’ range) [2, 3].

The challenge of acquiring complete NDE/SHM based damage characterization for aerospace composites is compounded not only by the complexity of the damage types occurring in composites, but also by the complex geometries of composite components required for aerospace applications. In recent years the aerospace community has increased the use of composites in aeronautic and space vehicles. Additionally, as demonstrated by NASA’s Composite Crew Module study (see figure 1), there is a push toward use of composites for primary structural components [4]. Thus, damage characterization techniques are required for components such as composite joints.



Figure 1. Image of NASA Composite Crew Module pressure vessel, showing an example of a complex geometry CFRP aerospace composite structure [4].

The factors discussed previously lead to a need for realistic NDE and SHM simulation tools. Simulation tools have the potential to create a cost-effective method for developing and optimizing damage characterization techniques for composites. Additionally, such tools enable a method for predicting inspectability of advanced composite components during the design stage. For example, simulation tools could be used to establish confidence in an NDE or SHM technique's ability to inspect complex joints, hard to reach locations, and/or to inspect large areas. Having such information available during the design stage would allow for avoidance of 'uninspectable' designs, or, as is more likely, will allow for more lead-time in developing new inspection techniques when traditional methods are found to be inadequate. Commercial-off-the-shelf (COTS) NDE simulation software is not currently adequate for simulating energy interaction with realistic defects in 3-dimensional (3D) composite laminates and complex geometry composite components at the large size scales required for aerospace applications. Furthermore, realistic and rapid simulation tools will likely be required to validate large-area-coverage SHM systems since it would be unfeasible and costly to rely solely on experimental methods to establish a probability of detection for all possible defect locations, geometries, and types. The lack of adequate validation methodologies for SHM systems remains a key issue that must be tackled before SHM systems can be fully utilized on aeronautic and space vehicles. Prior authors have utilized models in SHM reliability assessments, but there is still significantly more progress needed in this area [5]. NASA's future long duration manned spaceflight missions will benefit, in particular, from validated autonomous SHM systems.

As cost-effective high performance computational resources (such as many-integrated-core and graphics processing unit architectures) continue to become more readily available, the development of such simulation tools, and the related capabilities that will be enabled, are expected to eventually lead to a shift in the process flow of aerospace composite design. Figure 2 (left) shows a concept diagram of the current design to in-service inspection process flow which does not utilize simulations at the design stage, full damage characterization, or validated SHM. Figure 2 (right) also shows a possible future process flow concept that leverages simulation tools and the technologies/methodologies that simulation tools can enable (including SHM).

Ultrasound-based NDE is a common technique for damage detection in composite materials. Additionally, ultrasonic guided wave methods are a promising technique for SHM due to their ability to cover large areas with few sensors [6]. This paper describes the development and implementation of a custom 3D ultrasound simulation tool that models ultrasonic wave interaction with realistic 3D damage in CFRP composites. The custom code uses elastodynamic finite integration technique (EFIT) and is parallelized to run efficiently on computing cluster or multicore machines. The following section will provide background on NDE and SHM simulation approaches, as well as providing details of the EFIT approach for composites and the benefits of using custom code. The remainder of the paper discusses example applications of the simulation tool for investigating wave interaction with damage in composite materials, including delaminations and microcracking. The intention is to give an overview of ongoing ultrasound simulation work pushing toward realistic 3D simulations for complex composites.

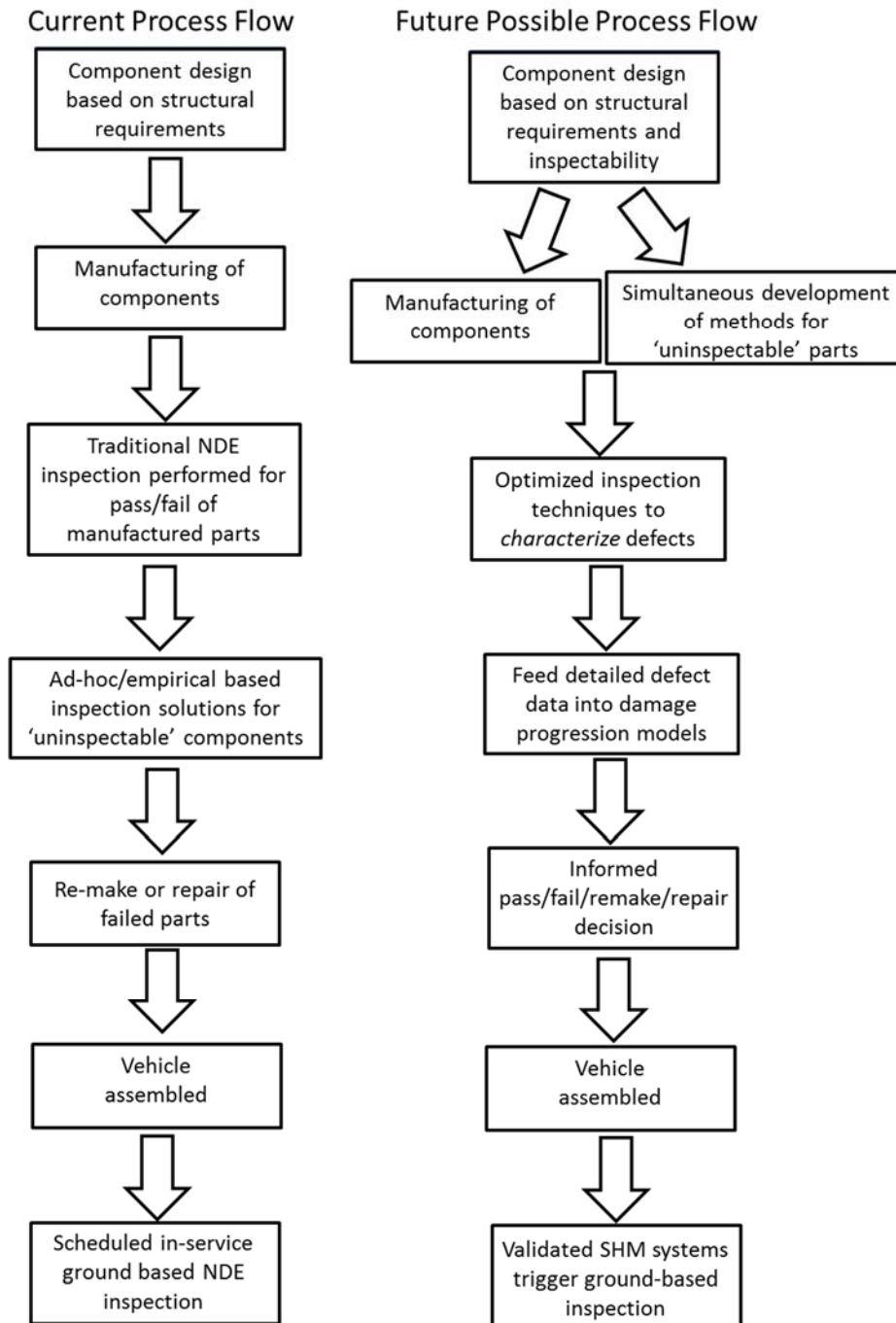


Figure 2. Left: Diagram showing current design-to-vehicle process flow that does not include NDE/SHM simulation tools, full damage characterization, or SHM. Right: Possible future design-to-vehicle process flow that leverages simulation tools and the methodologies simulation can enable.

ULTRASOUND SIMULATION IN NDE AND SHM

A number of mathematical approaches have been used over the last several decades for numerical simulation of ultrasonic wave propagation in materials, including finite element analysis (FEA), finite difference (FD), and finite integration technique (FIT). Many FEA based commercial software packages exist for simulating

physics phenomena in materials/structures. In the scientific literature numerous authors use commercial FEA software to investigate ultrasonic wave behavior for damage detection in aerospace materials, including metals and composites. In recent years, several authors have reported simulation based investigations of both ultrasonic NDE and guided wave SHM for composites. Ramadas et. al. used 2D FEA via ANSYS to study guided waves and turning modes in a glass/epoxy T-joint [7]. Delrue et. al. used 3D FEA via Comsol to study wave interaction with a single circular delamination in a CFRP composite plate, including nonlinear delamination clapping behavior [8]. Liu et. al. used 3D FEA to study wave interaction with a single rectangular delamination in a CFRP composite plate [9].

These, and other prior reported work, demonstrate the usefulness of simulation tools for understanding and developing damage detection techniques for composites. However, these examples also demonstrate how most prior works in the literature is limited to either simplified 2D simulations (especially for complex geometries parts, i.e., non-plates), or are 3D but make simplifying assumptions about the damage geometry. More realistic simulations are needed to enable: 1) inspection predictability at design stage, 2) ‘full’ damage characterization techniques for aerospace composites, and 3) validation methods for SHM. The following section describes custom 3D EFIT simulation code which can incorporate 3D complex composite damage geometries. Additionally, as discussed further at the end of the paper, current work is focused on expanding the code to accurately model wave propagation in complex geometry composite components (while accounting for ply-level material properties).

Elastodynamic Finite Integration Technique for Composites

Elastodynamic finite integration technique is a numerical method similar to staggered-grid finite difference techniques. The technique has been in use since the early 1990s with extensive foundational work reported by authors such as Fellingner, Marklein, and Schubert, among others [10-12]. Most prior 3D EFIT work reported in the literature focused on simulating wave propagation in metals [13-15]. In recent years the Nondestructive Evaluation Sciences Branch (NESB) at NASA Langley Research Center has been working to develop custom 3D EFIT code for accurately modeling ultrasound in realistic aerospace composites. The extension of EFIT from metallic materials to composites leads to a significantly lengthier general form of the discretized equations [16]. For the most general case of anisotropic materials (triclinic), the stiffness matrix contains up to 21 different non-zero elastic constants [17]. For orthotropic materials this number decreases to 9 elastic constants. CFRP layups used for aerospace applications may fall into the orthotropic category, but more commonly (as in quasi-isotropic layups) will require more than 9 constants in the stiffness matrix to account for rotated ply layers. The custom EFIT code accounts for the material properties of each individual ply by including appropriate stiffness matrices for each ply rotation. The current code cannot account for woven composite materials, but rather, models unidirectional prepreg based layups that are common in aerospace applications.

The custom code has several benefits over commercial software. The code is written in C++ and is parallelized to run efficiently on cluster or multicore computing resources using Message Passing Interface (MPI). Additionally, the memory usage requirements are directly controlled and minimized. These two factors allow for

larger simulation sizes than would be feasible using most commercial software (the largest EFIT simulation implemented at NASA NESB to date was on the order of 1.8 billion grid cells, with tracking 9 variables at each grid cell). The custom code is ideal for adapting to new computational resources, such as graphics processing units (GPUs) and many-integrated-core (MIC) architectures. Porting the code to GPU and MIC resources is an area of ongoing work at NASA NESB. The code is also readily adaptable to include additional physics by directly altering the EFIT equations. Examples of the form of the discretized EFIT equations in Cartesian coordinates for composite materials are shown below. In particular, the v_x velocity equation and the T_{xx} normal stress are shown below (the additional 2 velocity equations, 2 normal stress equations, and 3 shear stress equations are not listed due to their extensive length, but can be found in [16]):

$$\dot{v}_x^{(n)}(t) = \frac{2}{\Delta x(\rho^{(n)} + \rho^{(n+\hat{x})})} \left[T_{xx}^{(n+\hat{x})}(t) - T_{xx}^{(n)}(t) + T_{xy}^{(n)}(t) - T_{xy}^{(n-\hat{y})}(t) + T_{xz}^{(n)}(t) - T_{xz}^{(n-\hat{z})}(t) \right] + g_1 \quad (1)$$

$$\begin{aligned} \dot{T}_{xx}^{(n)}(t) = & \frac{1}{\Delta x} \left[C_{11} \left(v_x^{(n)}(t) - v_x^{(n-\hat{x})}(t) \right) + C_{12} \left(v_y^{(n)}(t) - v_y^{(n-\hat{y})}(t) \right) + \right. \\ & C_{13} \left(v_z^{(n)}(t) - v_z^{(n-\hat{z})}(t) \right) + \frac{1}{4} C_{14} \left(v_y^{(n+\hat{z})}(t) + v_y^{(n-\hat{y}+\hat{z})}(t) - \right. \\ & v_y^{(n-\hat{y}-\hat{z})}(t) - v_y^{(n-\hat{z})}(t) + v_z^{(n+\hat{y}-\hat{z})}(t) + v_z^{(n+\hat{y})}(t) - v_z^{(n-\hat{y}-\hat{z})}(t) - \\ & v_z^{(n-\hat{y})}(t) \left. \right) + \frac{1}{4} C_{15} \left(v_x^{(n-\hat{x}+\hat{z})}(t) + v_x^{(n+\hat{z})} - v_x^{(n-\hat{x}-\hat{z})}(t) - v_x^{(n-\hat{z})}(t) + \right. \\ & v_z^{(n+\hat{x}-\hat{z})}(t) + v_z^{(n+\hat{x})}(t) - v_z^{(n-\hat{x}-\hat{z})}(t) - v_z^{(n-\hat{x})}(t) \left. \right) + \\ & \frac{1}{4} C_{16} \left(v_x^{(n-\hat{x}+\hat{y})}(t) + v_x^{(n+\hat{y})} - v_x^{(n-\hat{x}-\hat{y})}(t) - v_x^{(n-\hat{y})}(t) + v_y^{(n+\hat{x}-\hat{y})}(t) + \right. \\ & \left. v_y^{(n+\hat{x})}(t) - v_y^{(n-\hat{x}-\hat{y})}(t) - v_y^{(n-\hat{x})}(t) \right) \left. \right] \end{aligned} \quad (2)$$

With

$$v_i^{(t)} = v_i^{(t-1)} + \dot{v}_i^{(t-\Delta t/2)} \Delta t, \quad T_{ij}^{(t+\Delta t/2)} = T_{ij}^{(t-\Delta t/2)} + \dot{T}_{ij}^{(t)} \Delta t \quad (3)$$

$$\Delta t \leq \frac{\Delta x}{c_{max} \sqrt{3}}, \quad \Delta x \leq \frac{c_{min}}{10 f_{max}} \quad (4)$$

In equations (1) and (2): Δx is the spatial step size (a cubic Cartesian grid is assumed), ρ is the density of the material, C_{ij} are corresponding elements from the stiffness matrix for that ply layer (where $i=1:6$ and $j=1:6$), T_{ij} are shear and normal stresses (and dot notation \dot{T} denotes the time derivative of the corresponding variable), v_i is velocity in the \hat{i} direction, the notation $(n+\hat{i})$ means one spatial step in the \hat{i} direction past the current grid position, n , and \mathbf{g} is an external source (excitation). In equations (3) and (4): c_{min} and c_{max} are the minimum and maximum speeds of sound, f_{max} is the maximum frequency, and Δt is the time step size. Code validation studies and additional discussion about EFIT for composites can be found in prior work by the authors [18].

SIMULATIONS WITH REALISTIC CFRP DAMAGE

The custom code also has the benefit of easy incorporation of realistic composite damage. In prior work we have directly incorporated X-ray microfocus computed tomography (CT) data for real composite damage into the EFIT simulations [18-19]. Figures 3 and 4 show examples of real composite damage geometries taken directly from X-ray CT data and mapped into the ultrasound simulation. In both cases the damage was simulated by implementing stress free boundaries at each grid cell identified as damage by the X-ray CT damage data map. Figure 3 shows X-ray CT microcrack data (top) and an image from an EFIT simulation of bulk wave interaction with microcracking in a CFRP composite (bottom). In the X-ray CT microcrack data, the black outer regions are air outside the composite sample. White regions are pristine (non-cracked) regions of the sample, and black regions within the white are microcracks. The bottom image shows a single snapshot in time from the 3D EFIT simulation of wave interaction with the real microcrack geometries taken from the X-ray CT data. The excitation is in the center of the simulated sample, and the waves are extremely scattered due to the extensive microcracking throughout the volume of the simulated sample. Surface breaking microcracks can be observed as black streaks on the surface of the simulated sample.

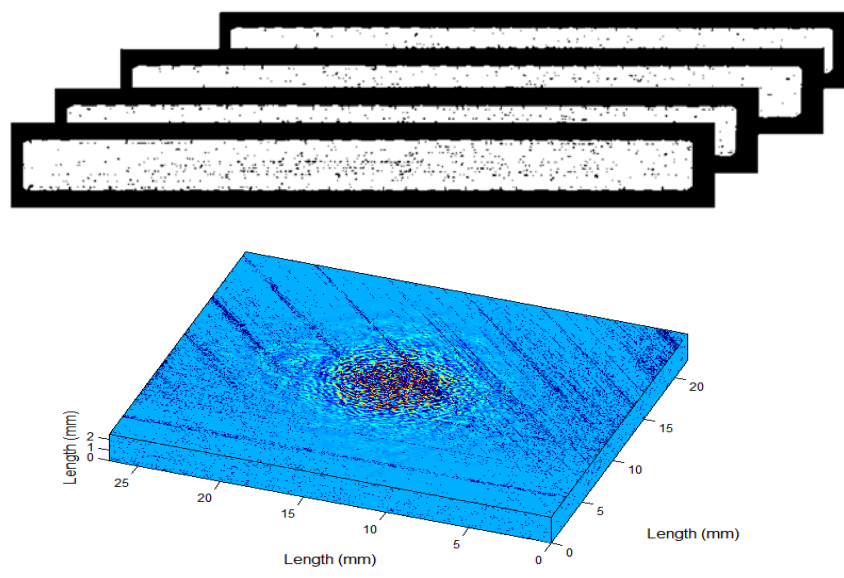


Figure 3. Top: Image slices from X-ray CT data damage map for a CFRP sample with microcracking. Bottom: Single snapshot in time from a 3D EFIT simulation of bulk wave interaction with the real microcrack geometries taken from the X-ray CT data. The images are further explained in the text.

Figure 4 shows X-ray CT data of an impact-induced delamination in a CFRP composite and an image from an EFIT simulation of guided wave interaction with the delamination damage. The X-ray CT data damage map (top) shows that the impact induced damage is a complex geometry multiply delamination. The damage map in figure 4 shows only the delamination (it does not show any surrounding pristine material). The bottom image shows a single snapshot in time from the 3D EFIT simulation of guided wave interaction with the real delamination geometry taken from the X-ray CT data. A circular excitation source is located at approximately $x=5$ mm

and $y = 80$ mm (top left corner), and the delamination is located at approximately $x = 40$ mm and $y = 50$ mm. In the EFIT image the colormap shows the velocity amplitude, where dark red indicates the largest positive ($+\hat{z}$) out-of-plane velocity amplitude and dark blue indicates the largest negative ($-\hat{z}$) out-of-plane velocity. Complex wave behavior, including mode conversion, can be observed as the waves pass above delaminated plies. Edge scattering occurs at the simulated sample edges.

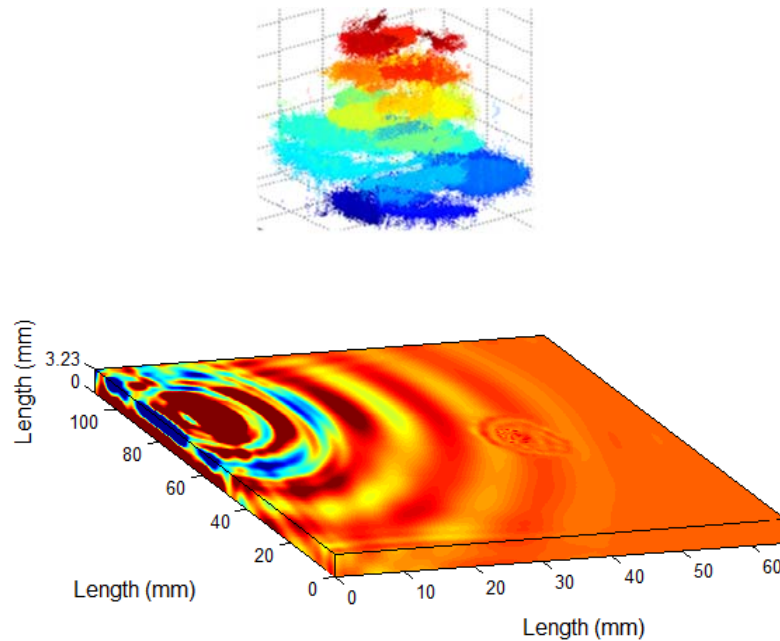


Figure 4. Top: Image slices from X-ray CT data damage map for a CFRP sample with delamination damage. The colors are provided as an aid to differentiating depths. Bottom: Single snapshot in time from a 3D EFIT simulation of guided wave interaction with the real delamination geometry taken from the X-ray CT data. The excitation source is located at $x = 5$ mm, $y = 80$ mm. The delamination is centered at approximately $x = 40$ mm, $y = 50$ mm.

Example of In-plane and Out-of-plane Guided Wave Interaction with Damage

One benefit of the 3D EFIT code is that since both in-plane and out-of-plane wave behavior are calculated, both can be output from the simulation (for all spatial locations throughout the simulated specimen). Since individual guided wave modes have varying displacement throughout the thickness of a material, certain modes may be better suited than others for detecting delaminations at various depths. Figure 5 shows out-of-plane and in-plane (v_x) motion at a single point in time for two different depths in the simulated delamination case. As in figure 4, the color map shows the velocity amplitude where dark red represents the largest positive velocity and dark blue represents the largest negative velocity. As shown in the images in figure 5a, at the top surface of the composite the out-of-plane guided wave interaction with the delamination creates a more clear indication of the damage location and size (where 'size' is the in-plane area of damage) than the in-plane wave interaction. Mode conversion (from the fastest symmetric guided mode to an antisymmetric mode) leads to more significant out-of-plane motion above the delamination damage at the

composite surface. Note that due to the complex shape and multilayered characteristic of the delamination damage, the behavior of waves as they pass above the damage region leads to more complicated wavenumber changes than the emergence of a single new mode wavenumber (as would be the case for a single ply depth ‘ideal’, and less realistic, delamination). The images in figure 5b show out-of-plane and in-plane wave behavior at a depth within the composite thickness that corresponds to the depth containing the largest amplitude of in-plane motion (approximately at mid-plane, i.e. midway through the sample thickness). At this depth the delamination occurring at that ply layer is observed in the images as black regions (void/air) located in the damage region. The images show larger amplitude in-plane motion near the damage region at this depth compared to the out-of-plane result. Thus, one can envision that if delamination damage were to occur only at this single depth, the out-of-plane waves would show little response to the damage presence. For this real delamination damage case, which spans much of the composite thickness, the mode conversion above the damage region at the composite surface (where any measurements would occur) in the out-of-plane result is likely the most useful wave information for characterizing the damage. Prior work by the authors has explored advanced data processing methods for analyzing the out-of-plane motion in order to characterize delamination damage [20].

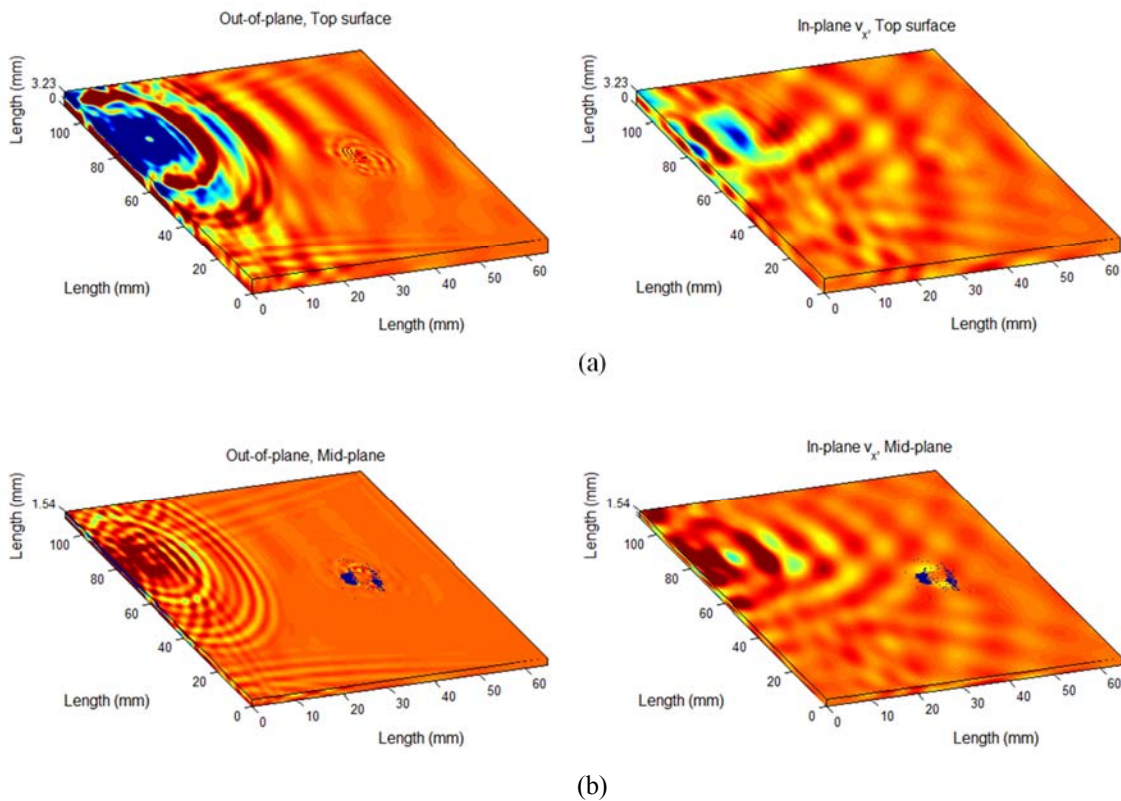


Figure 5. EFIT output at a single snapshot in time: (a) for the entire top surface of the composite for both out-of-plane and in-plane motion (as labeled); (b) Out-of-plane and in-plane motion (as labeled) at a depth approximately mid-way through the composite sample thickness. The excitation source is located at $x=5$ mm, $y=80$ mm. The delamination is centered at approximately $x=40$ mm, $y=50$ mm.

COMPLEX GEOMETRY COMPOSITES

FEA software can model wave propagation in 3D complex geometry components; however, current COTS software is not adequate for modeling realistic defects in 3D complex geometry composite components at the large size scales required for aerospace applications, especially at the computational speeds that will be required for utilizing simulation tools for the applications discussed in the introduction. Work is underway to expand the custom EFIT code to realistically model wave propagation and interaction with damage in complex geometry CFRP composites. The goal is to account for both ply level material property changes due to the layup and the changes in directionality of plies (and stiffness matrices) due to ply bends/curves, etc. Figure 6 shows a diagram of a composite T-joint. For plies in the skin and in the T stiffener, the stiffness matrices must be rotated in the x-y plane to account for the composite layup. In the curved region of the joint (where the T meets the skin) additional stiffness matrix rotation in the y-z plane is required to accurately model waves in that region. Ply-level fiber waviness (i.e., ‘ply waviness’) could also be incorporated via appropriate rotations of the stiffness matrix. Useful 3D complex geometry composite component simulations require larger size scales and more memory than the CFRP plate examples described above. This is an area where the custom, memory efficient simulation code is expected to be ideal.

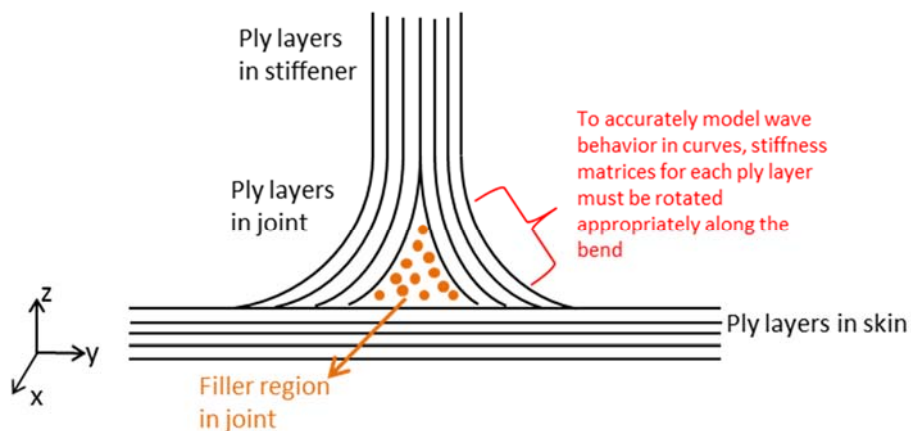


Figure 6. Diagram of a composite T-joint showing a T stiffener attached to a 4 ply thick CFRP skin. The diagram shows details that must be accurately captured in 3D NDE/SHM ultrasound simulations, including material properties of the filler region, material properties for each ply layer in the skin and T to capture layup, and material properties as plies bend in curved regions (requiring ply rotation both to capture layup and geometry).

CONCLUSION

This paper reviewed ongoing NDE and SHM simulation tool development at NASA NESB. A vision of the potential impact of realistic simulation tools for NDE and SHM was described, including possible changes to the process flow for aerospace vehicle/component design through in-service inspection. The paper gave an overview of progress toward realistic 3D ultrasound simulations for aerospace composites, including examples incorporating realistic composite damage and a discussion of steps

currently underway for expanding the custom code to accurately model complex geometry composite components. The custom EFIT code provides numerous benefits, as described above, and is expected to be an ideal route for expansion of NASA's ultrasonic NDE and SHM simulation tools.

REFERENCES

1. Canturri, C., Greenhalgh, E., Pinho, S., Ankersen, J. 2013, "Delamination growth directionality and the subsequent migration processes—The key to damage tolerant design." *Composites Part A: Applied Science and Manufacturing* 54: 79-87.
2. Roberts, R.A., and Leckey, C.A.C., 2013, "Computational modeling of micro-crack induced attenuation in CFRP composites." *Review of Progress in Quantitative Nondestructive Evaluation* 32: pp 979-986.
3. Yurgartis, S. W. 1987, "Measurement of small angle fiber misalignments in continuous fiber composites." *Comp Sci Technol* 30(4): 279-293.
4. NASA NESC, 2010, "Composite Crew Module Pressure Vessel Pathfinder Development", http://www.nasa.gov/offices/nesc/home/Feature_CCM.html#U0MNRxBnB8F (date last accessed: 4/7/2014)
5. Aldrin, J. C., Medina, E. A., Lindgren, E. A., Buynak, C. F., & Knopp, J. S. 2011, "Protocol for reliability assessment of structural health monitoring systems incorporating model-assisted probability of detection (MAPOD) approach" Technical Report, Air Force Research Lab Wright Patterson AFB OH. ADA585081
6. Tian, Z., Leckey, C., Yu, L. 2013, "Damage Detection in Composite Structures With Wavenumber Array Data Processing". *ASME Conference on Smart Materials, Adaptive Structures and Intelligent Systems* (pp. V002T05A015-V002T05A015). American Society of Mechanical Engineers.
7. Ramadas, C., Balasubramaniam, K., Joshi, M., & Krishnamurthy, C. V. 2011, "Interaction of Lamb mode (A_0) with structural discontinuity and generation of 'Turning modes' in a T-joint". *Ultrasonics*, 51(5):586-595.
8. Delrue, S., & Van Den Abeele, K. 2012, "Three-dimensional finite element simulation of closed delaminations in composite materials". *Ultrasonics*, 52(2): 315-324.
9. Liu, Z., Yu, H., He, C., & Wu, B. 2013, "Delamination detection in composite beams using pure Lamb mode generated by air-coupled ultrasonic transducer". *J Intell Mater Sys Struct*, 1045389X13493339.
10. Fellingner, F. and Langenberg, K.J., 1990, "Numerical techniques for elastic wave propagation and scattering", in *Elastic Waves and Ultrasonic Nondestructive Evaluation*, edited by S.K. Datta, J.D. Achenbach, and Y.S. Rajapakse, Elsevier, North-Holland, Amsterdam, pp. 81-86.
11. Marklein, R., Barmann, R. and Langenberg, K.J., 1995, "The Ultrasonic Modeling Code EFIT as Applied to Inhomogeneous Dissipative and Anisotropic Media", in *Review of Progress in Quantitative Nondestructive Evaluation 14B*, edited by D.O. Thompson and D.E. Chimenti, Plenum Press, NY, pp. 251-258.
12. Schubert, F., Peiffer, A. and Kohler, B., 1998, "The Elastodynamic Finite Integration Technique for Waves in Cylindrical Geometries", *J Acoust Soc Amer* 104:pp. 2604-2614.
13. Rudd, K. E., Leonard, K. R., Bingham, J. P., Hinders, M. K., 2007, "Simulation of guided waves in complex piping geometries using the elastodynamic finite integration technique". *J Acoust Soc Amer*, 121(3):1449-1458.
14. Bingham, J., Hinders, M., 2009, "Lamb wave characterization of corrosion-thinning in aircraft stringers: Experiment and three-dimensional simulation". *J Acoust Soc Amer*, 126(1):103-113.
15. Bingham, J., Hinders, M., 2010, "3D elastodynamic finite integration technique simulation of guided waves in extended built-up structures containing flaws". *J Comput Acous*, 18(2): 165-192.
16. Halkjaer, S., 2000, "Elastic Wave Propagation in Anisotropic Inhomogeneous Materials", Ph.D. dissertation, Technical University of Denmark, Lyngby Denmark.
17. Rose, J. L., 2004, *Ultrasonic waves in solid media*. Cambridge university press.
18. Leckey, C.A.C., Rogge, M. D., & Raymond Parker, F., 2014, "Guided waves in anisotropic and quasi-isotropic aerospace composites: Three-dimensional simulation and experiment". *Ultrasonics*, 54(1):385-394.

19. Leckey, C.A.C., Rogge, M. and Parker, R., 2013, "Microcracking in composite laminates: Simulation of crack-induced ultrasound attenuation". *Review of Progress in Quantitative Nondestructive Evaluation*, 32:947-954.
20. Leckey, C. A.C., Parker, F. R., 2014, "Simulation based investigation of hidden delamination damage detection in CFRP composites". *Review of Progress in Quantitative Nondestructive Evaluation*, 1581(33):1114-1129.